Solid Freeform Fabrication 2024: Proceedings of the 35th Annual International Solid Freeform Fabrication Symposium – An Additive Manufacturing Conference
Reviewed Paper

The Impact of Different HIP Treatment Cycles on Fatigue Behavior during 4-Point Bending of Additively Manufactured (AM) Ti-6Al-4V

D.A. Ariza[1,3], E. Arrieta[1,2], C. Banuelos[1,2], B. Colón[1,2], R.B. Wicker[1,2], C. Beamer[4], F. Medina[1,2]
[1] W. M. Keck Center for 3D Innovation, The University of Texas at El Paso, El Paso, TX 79968, USA,
[2] Department of Aerospace and Mechanical Engineering, The University of Texas at El Paso, El Paso, TX 79968, USA,
[3] Department of Metallurgical, Materials, and Biomedical Engineering, The University of Texas at El Paso, El Paso, TX 79968, USA,
[4]Quintus Technologies, 8270 Green Meadows Drive North, Lewis Center, OH 43035, USA

*Corresponding author: (daarizabarb@miners.utep.edu)

Abstract

The fatigue behavior of additively manufactured (AM) Ti-6Al-4V has been widely investigated under axial loading, with limited analysis of its performance under bending conditions. Internal defects in AM parts can detrimentally affect the integrity of 3D-printed specimens, impacting their fatigue performance. Researchers have previously implemented the Hot Isostatic Pressure (HIP) post-processing method to address the presence of defects. This study explores the fatigue life of Laser Powder Bed Fusion (L-PBF) Ti-6Al-4V after three HIP treatments: standard, low temperature/high pressure (LTHP), and super beta HIP, alongside annealed heat treatment. Optical techniques were utilized to assess microstructure, while tensile and hardness testing examined mechanical properties. Fracture morphologies and stress-life (S-N) curves were analyzed to understand fatigue behavior. Initial findings indicate that specific HIP post-processing can enhance the fatigue performance of Ti-6Al-4V under 4-point bending.

1. Introduction

Additive Manufacturing (AM), commonly known as 3D printing, has become a widely used technology in the last years. Several fields of applications including aerospace, industrial, automotive, and biomedical, have used the advances and advantages of this technology to fulfill their goals [1–7]. Across the different laser-based AM technologies, Laser Powder Bed Fusion (L-PBF) also know as Selective Laser Sintering (SLM) or Direct Metal Laser Sintering (DMLS), has become one of the most popular approaches. L-PBF is defined as an AM process in which thermal energy selectively fuses regions of a powder bed on a layer-by-layer basis [8–10]. L-PBF can provide a wide range of advantages in comparison to other AM technologies, for example, new degrees of freedom in design, higher resolution than other laser-based systems, creation of detailed and fine features, reduced surface roughness, reduction of manufacturing time, mass production, and the presence of high cooling rates that can lead to refined microstructure and enhancement of mechanical properties [9,11–13].

There are still some limitations with the use of AM technologies such as L-PBF, for example the presence of internal defects and porosity. Porosity can be present in different ways, for example bubble gas entrapment, which is directly related to the precursor powder particles, keyhole, and even lack-of-fusion (LoF) porosity directly related to a poor selection of process parameters

[14,15]. However, even though the selected printing parameters fall under the process window region of a material, also known as nominal parameters, still the presence of porosity can be present on the 3d printed specimens. It has been well reported [16–19] that the presence of defects and porosity can detrimentally affect the integrity of the 3d printed specimens and can lead to an earlier failure especially if mechanical testing such as fatigue is taking place by acting as stress concentrators and initiation sites. Because of this, it is important to develop 3D printed specimens without the presence of these anomalies.

The use of Hot Isostatic Pressing (HIP) type of heat treatment that involves heating a metal component at a high temperature under continuous isostatic pressure can be implemented to enhance densification and reduce porosity in AM builds [20,21]. In the same way, the use of HIP post-processing not only increases density and eliminates porosity, but also literature has shown promising results in which this improves the fatigue strength and mechanical properties of specimens. For example, in a recent study, Hills et al. [22], investigated the effects of chemical etching on the fatigue failure of L-PBF Ti-6Al-4V specimens subjected to either heat treatment or HIP. The results revealed that HIP treatment effectively closed most internal pores, significantly enhancing fatigue behavior. The HIP treated specimens exhibited fatigue performance comparable to that of wrought Ti-6Al-4V. Zhao et al. [23], compared the microstructures and mechanical properties, including the fatigue performance, of Ti-6Al-4V fabricated by selective laser melting (SLM) and electron-beam melting (EBM). They found that HIP treatment significantly improved the fatigue performance of both laser-based technologies compared to as-built specimens. The study also reported that HIP treatment not only closed most internal pores but also altered the microstructure of Ti-6Al-4V, affecting its mechanical properties such as strength and ductility. Yu et al. [24] also investigated the impact of surface finishing, HIP, and heat treatments on the fatigue performance of SLM Ti-6Al-4V. They found that reducing or eliminating pores through HIP treatment significantly extended the fatigue crack initiation period and increased the specimens' fatigue limit, obtaining a superior performance compared to as built and heat-treated specimens. Alternatively, Moran et al. [25] examined the fatigue behavior of various HIP cycle treatments. Their findings suggested that neither microstructure nor the presence of defects primarily governs the fatigue performance of AM Ti-6Al-4V. However, they did not address the effects of HIP on the material's mechanical properties.

Research into the fatigue performance of Ti-6Al-4V has been extensive, primarily conducted under conventional uniaxial conditions [16,26–32], which are generally considered conservative. In contrast, there is a notable scarcity of literature on Ti-6Al-4V fatigue testing using the 4-point bending method. The 4-point bending approach offers a more realistic simulation for complex engineering system designs. Therefore, it is crucial to investigate and analyze this fatigue mechanism. Unlike the uniform stress distribution in uniaxial testing, 4-point bending concentrates maximum stress at the bottom surface of the beam between the inner support pins, as illustrated in Figure 1. As a result of these considerations, the primary objective of this study is to investigate the influence of three distinct HIP cycles on the fatigue characteristics of AM Ti-6Al-4V subjected to 4-point bending conditions.

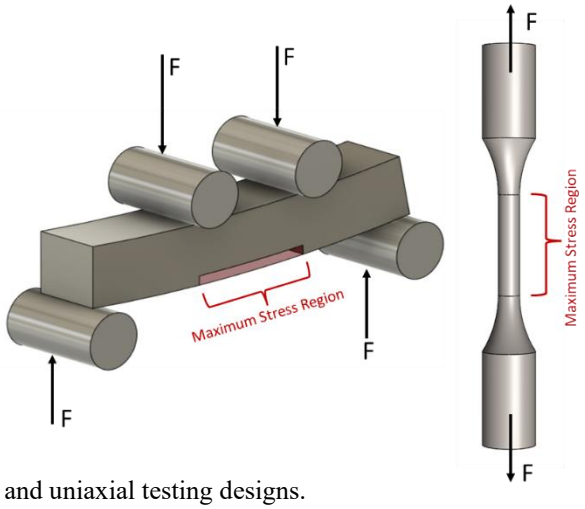

Figure 1. 4-point bending and uniaxial testing designs.

2. Materials & Methods

2.1. Powder Feedstock

In this study, commercial gas-atomized Ti-6Al-4V powder provided by Allegheny Technologies (ATI) was used. Figure 2 illustrates the powder's morphology, revealing regular spheres along with some irregular blocks. In the same way, the initial powder showed an average powder size distribution (PSD) with particle diameters of D10: 25 µm, D50: 37 µm, and D90: 49 µm. Additionally, the powder exhibited minimal porosity as can be seen in the as-polished image (Figure 3).

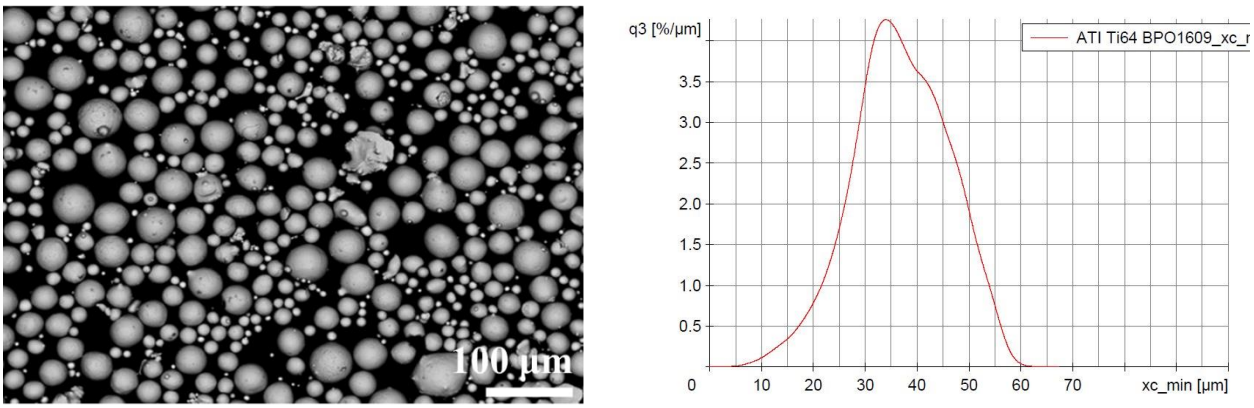

Figure 2. Gas-atomized ATI Ti-6Al-4V powder and particle size distribution curve.

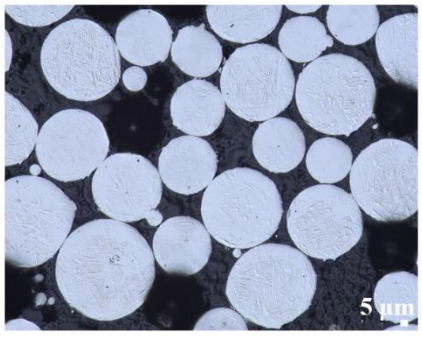

Figure 3. As-polished ATI Ti-6Al-4V powder optical image.

2.2. Process Parameters

The specimens in this study were fabricated using the commercial L-PBF system EOS M290, utilizing EOS nominal parameters: a laser power of 280 W and a scanning speed of 1200 mm/s. To prevent oxidation, the printing process was conducted in an argon-inert environment. Rectangular bars were first printed and then machined into 4-point bending specimens with a square cross-section (5 mm per side) and a height of 45 mm, featuring 45-degree chamfers. Machining is essential for L-PBF specimens, as as-printed surfaces often contain imperfections, defects, and residual stresses that can negatively impact fatigue performance. Therefore, machining is critical to achieve a high-quality surface finish, relieve residual stresses, and ensure consistent, accurate geometry in the specimens.

2.3. Heat Treatments

The 4-point bending specimens underwent the following heat treatments: Annealed, standard HIP, low temperature/high pressure (LTHP) HIP, and super beta HIP. For the standard HIP process, the parameters were set to 900°C and 100 MPa for 2 hours with natural cooling. The LTHP process used 815°C and 190 MPa for 2 hours, also followed by natural cooling. The super beta HIP process involved heating at 1050°C and 100 MPa for 1.5 hours, followed by rapid quench cooling. This was then followed by martensitic tempering within the HIP at 800°C for 2 hours under pressure, with natural cooling. Before any HIP treatments, all specimens were annealed at 600°C for 2 hours. All heat treatments were performed prior to final machining.

2.4. Metallographic Specimen Preparation and Microstructure Characterization

Metallographic specimens were mounted in a thermosetting mixture of black epoxy and phenolic powders in a 1:2 ratio. The preparation process began with grinding using P320 and P600 Sillicon Carbide (SiC) papers each for 3 minutes at a force of 25 N. This was then followed by pre-polishing with a 9 μm diamond suspension for 5 minutes at a force of 30 N, and concluded with a final mirror polishing using a solution of 0.1 μm eposil fumed colloidal silica for 10 minutes with the last 30 s using only water at a force of 40 N. The microstructure of the specimens was revealed by using Kroll's etchant consisting of a mixture of 91% deionized water, 6% nitric acid (HNO_3), and 3% hydrofluoric acid (HF). In addition to optical microscopy, advanced techniques like electron backscatter diffraction (EBSD) were employed to analyze the microstructure of the specimens.

2.5. Tensile & Hardness Testing

One specimen from each group was machined and tensile tested per ASTM E8-22 to provide a summary of the mechanical properties.

A micro-indentation hardness test was conducted according to ASTM E384 using the Vickers (HV) scale on a Qatm - Qness 30 CHD Master+. The measurements were taken with a load of one kgf (HV1), producing five indentations spaced three millimeters apart on the specimen surfaces. Each indentation had a dwell time of 15 seconds at room temperature.

2.6. Fatigue Testing

The 4-point bending fatigue testing was conducted using Minnesota, USA's MTS Landmark servo-hydraulic apparatus. This machine was equipped with a 10kN load cell and included a stainless-steel, adjustable 4-point bending unit provided by Material Testing

Technologies, Illinois, USA. Figure 4 presents a detailed setup of the MTS Landmark paired with the MTT's 4-point bending module. The testing parameters include a testing frequency of 10 Hz, maximum cycles up to 10^6, stress ratio (R) of 0.1, and inner and outer support distances of 10 mm and 30 mm, respectively.

Five different stress levels, including 100, 90, 80, 70, and 60% of the specimens' yield strength (reported in Table 2), were chosen to develop stress vs. fatigue life (S-N) curves ranging from 10,000 to 7,000,000 cycles. Implementing different stress levels provides a comprehensive understanding of the material's fatigue behavior, offering a more accurate representation of real-world service conditions.

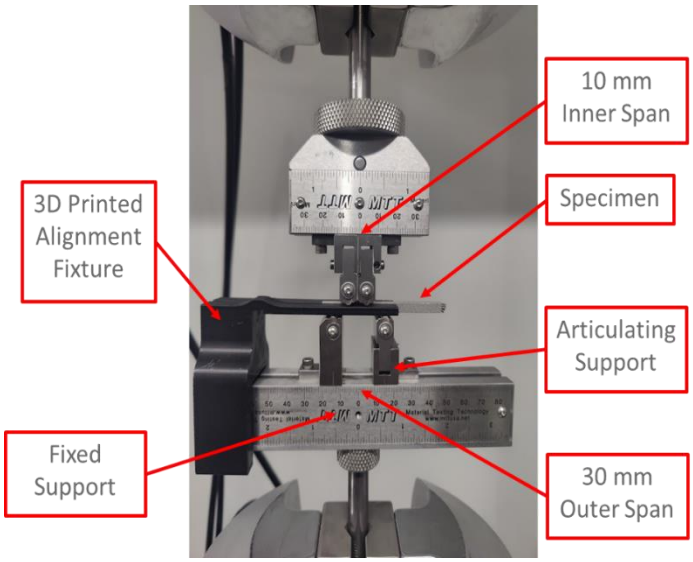

Figure 4. 4-point bending fatigue testing setup.

2.7. Fractography Analysis

The specimens' fracture surfaces were further analyzed with a JEOL JSM-IT500 Scanning Electron Microscope (SEM) to identify the fatigue crack initiation site (FCI), as well as the propagation and catastrophic rupture regions.

3. Results & Discussion

3.1. Microstructure

Figures 5 and 6 illustrate the microstructures of the different heat treatments in the XY and XZ planes. Looking first into the XZ planes (Figure 5), the annealed, standard HIP, and LTHP HIP specimens (Figures 5(a), 5(b), and 5(c)) display prior-β grains oriented along the build direction with epitaxial growth. In contrast, the super beta HIP specimen (Figure 5(d)) does not exhibit these elongated grains along the build direction. Instead, it shows coarse prior-β grains with an equiaxed morphology. A closer examination of the XY plane (Figure 6) reveals bundles of columnar grains in the annealed, standard HIP, and LTHP HIP specimens. Similar to the XZ plane, the super beta HIP specimen exhibits the presence of coarse prior-β grains.

A closer inspection of the annealed specimen (Figure 6(a)) reveals fine black lamellae, known as α' martensite, within the elongated and bundles of columnar grains. This microstructure forms due to the high cooling rates during the L-PBF process, which transforms

most of the β phase into the α' metastable phase [26,33,34]. Additionally, this microstructure is influenced by the annealing temperature; higher annealing temperatures can result in the formation of coarse α platelets [35]. This distinctive microstructure aligns with previous studies on L-PBF Ti-6Al-4V, highlighting the significant impact of high solidification rates [33,36–38].

Contrary to the annealed specimen, the HIP groups do not show the presence of the α' metastable phase in their microstructure. Instead, their microstructure primarily consists of the α + β dual phase. An important aspect to consider regarding the microstructure of the HIP groups is the temperature parameters and cooling rates involved during the specimens' thermal history. It is well-known that titanium, as an allotropic element, can exist in two different crystal structures depending on the β-transus temperature (~950˚C). Below this temperature, titanium is in the hexagonal close-packed (HCP) α-Ti phase, while above it, titanium is in the body-centered cubic (BCC) β-Ti phase [39]. Given the above, the phase transformation in Ti-6Al-4V is highly dependent on the temperature history and cooling rates induced by the fabrication process [39]. Examining the standard and LTHP HIP microstructures (Figures 5(b), (c) and 6(b), (c)), it is evident that their HIP cycles occurred below the β-transus temperature of Ti-6Al-4V (~950˚C). Literature suggests that HIP treatments below this temperature typically involve slow cooling rates, which prevent the formation of metastable α' martensite and instead lead to the formation of the α + β dual phase [40]. A closer examination of their microstructures (Figures 6(b) and (c)) reveals what appears to be the α + β Widmanstätten microstructure, characterized by a basket weave appearance. Additionally, the presence of α platelets (white regions), retained β matrix (dark lines), and α colonies is visible. A notable distinction between these two microstructures is the width of the α platelets. The standard HIP specimen displays wider α platelets, whereas the LTHP HIP specimen exhibits a finer microstructure.

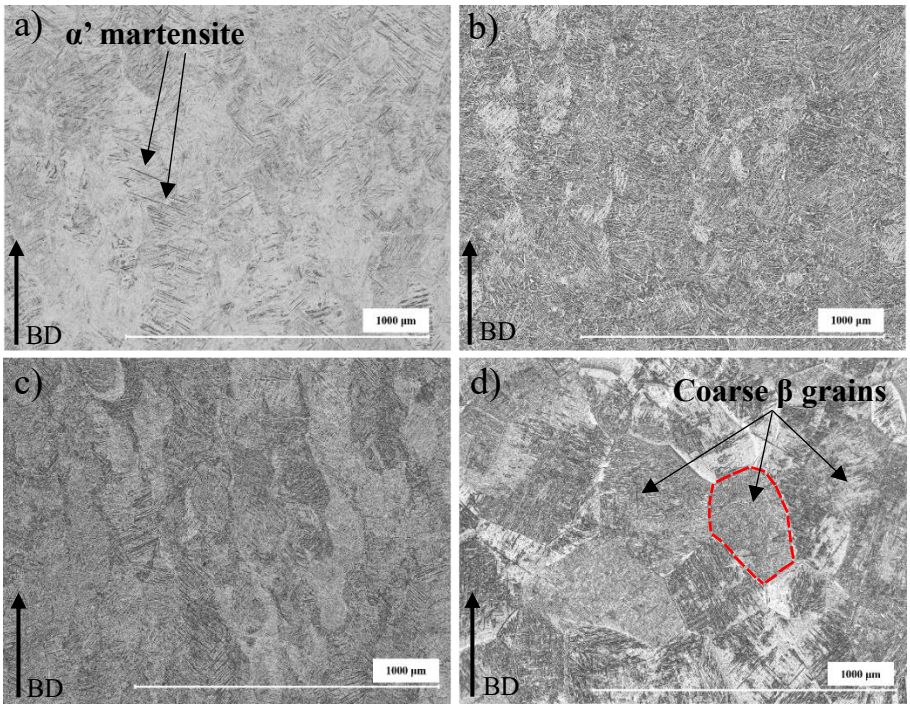

Figure 5. Ti-6Al-4V microstructures after heat treatments in plane XZ. a) Annealed. b) Standard HIP. c) LTHP HIP. d) Super Beta HIP.

Among the four different heat treatments, the most distinctive microstructure is observed in the super beta HIP specimen. For this specimen, the HIP temperature exceeds the β-transus temperature of Ti-6Al-4V (~950˚C), and its HIP cycle includes rapid quench cooling, resulting in fast cooling rates during its thermal history. Consequently, the super beta HIP microstructure is fully equiaxed with coarse β grains and features thin α platelets. This indicates recrystallization and the shearing of long columnar grains due to treatment above the β-transus [40–42].

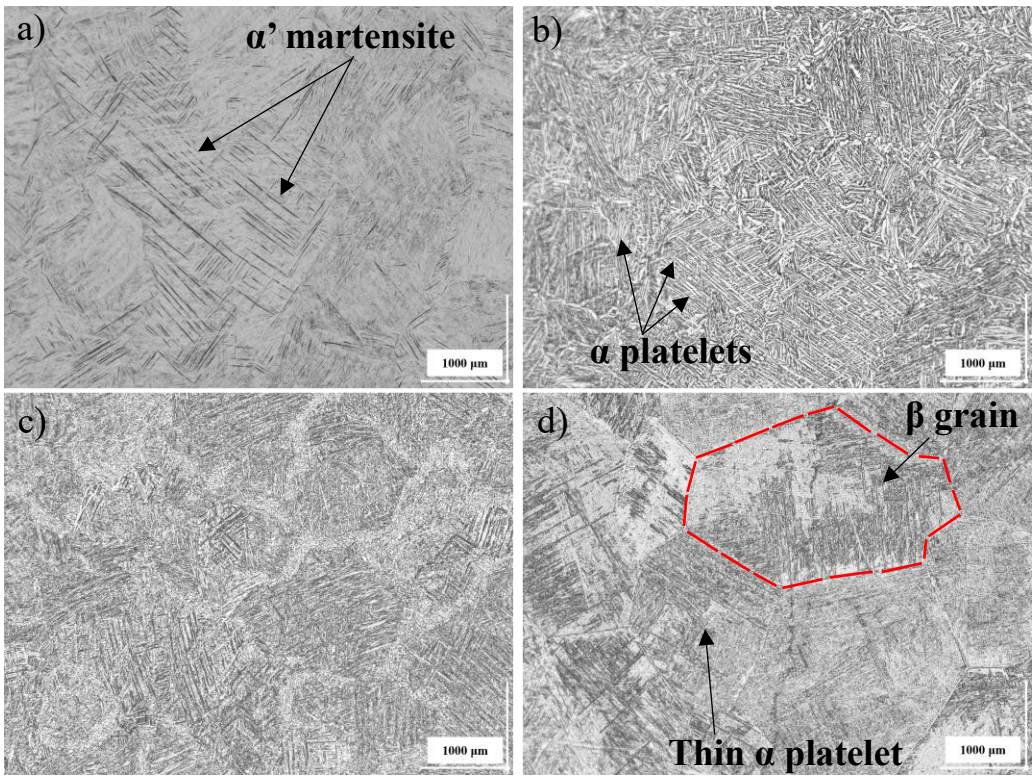

Figure 6. Ti-6Al-4V microstructures after heat treatments in plane XZ. a) Annealed. b) Standard HIP. c) LTHP HIP. d) Super Beta HIP.

Figure 7 shows the microstructure of the specimens after heat treatments analyzed by EBSD at the XZ planes of the 4PB specimens. The EBSD results confirmed the previously shown microstructural evolution of the heat treatments. The annealed specimen (Figure 8(a)) shows a well-defined α' martensite phase. Both standard and LTHP HIP specimens show (Figures 8(b) and (c)) refined α platelets. On the other hand, the super beta HIP (Figure 8(d)) reveals a more complex grain structure, where the transformation of β grains to coarse equiaxed instead of columnar can be evident, evidencing the effects of the HIP treatment cycle. It is important to mention that among the different heat treatments, the LTHP HIP specimen resulted in the highest percentage of low-angle grain boundaries (LAGB), indicating sub-grain formation in the microstructure. Literature has suggested that the presence of sub-grains can enhance fatigue performance by impeding crack initiation and propagation [43]. Table 1 summarizes the heat treatment specimens' low- and high-angle grain boundaries (HAGB).

Heat Treatment	*Low-angle grain boundaries (LAGB) (%)*	*High-angle grain boundaries (HAGB) (%)*
Annealed	2.07	97.9
Standard HIP	4.88	95.1
LTHP HIP	6.41	93.6
Super Beta HIP	1.46	98.5

Table 1. Low- and High-angle grain boundaries of heat-treated specimens from EBSD results.

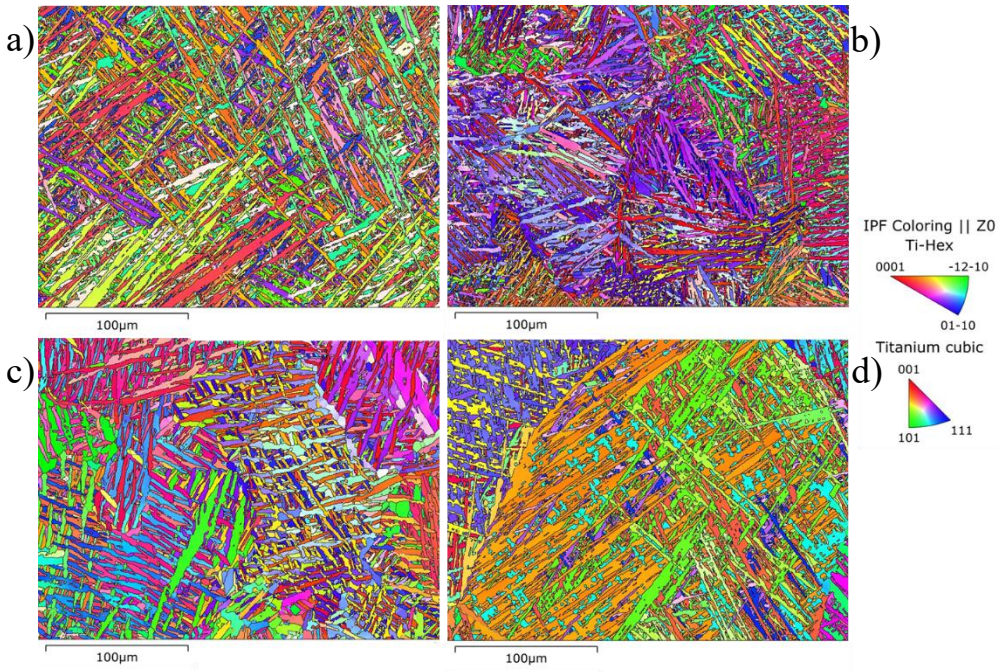

Figure 7. EBSD images showing the microstructure of the specimens after heat treatment. a) Annealed. b) Standard HIP. c) LTHP HIP. d) Super Beta HIP.

3.2. Mechanical Properties

Table 2 presents the mechanical properties of Ti-6Al-4V samples subjected to various heat treatments. The annealed sample exhibited the lowest elongation and modulus of elasticity, which can be attributed to the presence of α' martensite, known for its low ductility [26,33,42,44,45]. However, the same α' martensite also contributed to the annealed sample achieving the highest ultimate tensile strength (UTS), yield strength (σ_y), and Vickers hardness (HV) values, measuring 1298 MPa, 1227 MPa, and 395 HV1, respectively. In contrast, the hardness of the HIP-treated samples significantly decreased due to the presence of the softer α + β and weaker microstructure [37]. Consistent with several studies, the β phase in titanium alloys has the lowest microhardness values, explaining the observed results [46,47]. Similarly, the HIP specimens demonstrated higher elongation results, primarily due to the absence of α' martensite and the presence of the more ductile α + β microstructure. The HIP post-processing also yielded superior results for the modulus of elasticity, particularly in the standard HIP group, indicating greater resistance to deformation. Tensile and yield strength values observed in HIP-treated samples can also be attributed to the increased volume fraction of the ductile β phase, however, further analysis will be needed to draw any specific conclusions. Additionally, within the HIP groups, the tensile and yield strength improved as the size of the α phase

decreased, as seen in the LTHP HIP specimen, which exhibited a finer microstructure (Figures (5c) & (6c)).

Heat Treatment	***UTS (MPa)***	σ_y ***(MPa)***	ε_f ***(%)***	HV_1 $(kg_f mm^{-2})$
Annealed	1298	1227	9	395
Standard HIP	1032	959	14	346
LTHP HIP	1124	1047	16	342
Super Beta HIP	1041	942	14	347

Table 2. Tensile and hardness testing mechanical properties (0.2% offset yield strength).

3.3. Stress vs Fatigue (S-N)

The S-N results for the 4-point bending fatigue testing are presented in Figure 8. Throughout the testing, several specimens across the groups exhibited run-outs, indicating no evidence of fracture. Markers with arrows denote these run-outs after 7,000,000 cycles.

Analyzing the S-N curves (Figure 8), the annealed group exhibits superior performance compared to the HIP groups. Contrary to expectations from literature [48,49], which suggest that the presence of α' martensite reduces fatigue performance due to its propensity to promote fatigue crack initiation through high local stresses and brittleness, the annealed specimens performed better. A possible explanation for this superior performance than the HIP groups is attributed to the absence of defects serving as initiation sites. Additionally, these results align with previous studies, which indicate that harder specimens (395 HV1) with higher tensile strength exhibit improved fatigue performance [50].

Among the HIP groups, the LTHP group demonstrated the best fatigue results, followed by the standard and super beta HIP groups, which obtained just a few cycles to failure, across all group specimens. Although the number of defects detected in the HIP groups was similar, these defects did not seem to significantly reduce fatigue performance, particularly in the LTHP HIP group. It has been reported [28,51] that applying additional post-processing, such as HIP, significantly reduces the size of defects or nearly eliminates them, consequently delaying crack propagation. This indicates that the presence of inclusions or anomalies in the HIP groups only moderately affects the fatigue life of the specimens, underscoring the effectiveness and importance of HIP treatments for fatigue testing.

The fatigue results are consistent with the effects of the HIP cycles on the specimens' microstructures. Literature [25,52] indicates that HIP cycles above the β-transus temperature of Ti-6Al-4V result in a coarser microstructure, leading to poorer fatigue performance, as observed in the super beta HIP groups. Additionally, the high temperatures during the super beta HIP cycle may contribute to detrimental performance.

Conversely, HIP cycles below the β-transus temperature produce finer microstructures, improving fatigue life, as seen in the LTHP HIP group. Similar results have been reported in the literature [25,53,54], where low-temperature and high-pressure samples exhibit better fatigue behavior than other HIP cycles. The beneficial effect of temperature reduction and

increased pressure in enhancing fatigue life is evident. The presence of thin α platelets acts as barriers to dislocation movement, hindering crack propagation, thereby increasing strength and improving fatigue resistance.

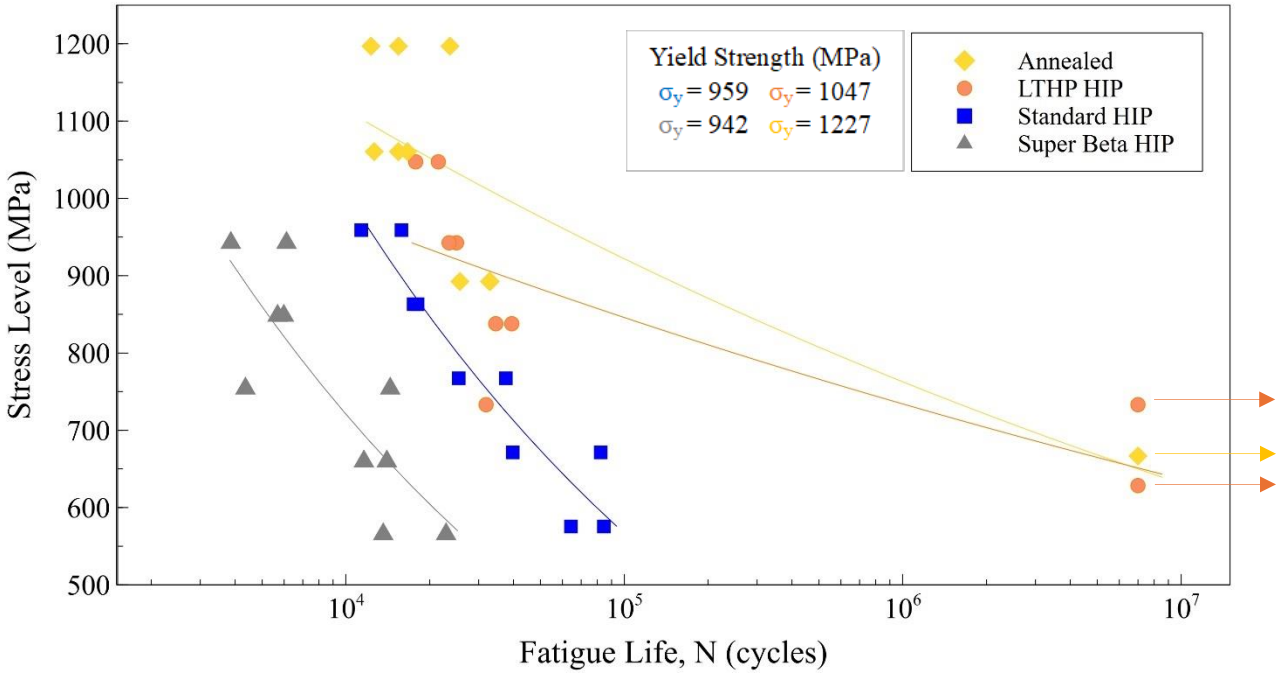

Figure 8. Stress vs Fatigue Life 4-point bending testing. Markers with arrows denote runoffs.

3.4. Fractography

Fracture morphologies of the 4-point bending are shown in Figure 9. In here, initiation sites, propagation regions, and catastrophic regions have been denoted within the fractography images. The annealed specimen (Figure 9(a) and (b)) shows an initiation site coming directly from the bottom surface. Fatigue striations can be seen spreading across the specimen. Figure 9(c) displays a fatigue crack initiation (FCI) site near the surface of the standard HIP specimen. Upon closer microscopic examination of the highlighted region, striation marks are observed, indicating that a surface anomaly likely acted as the origin of failure (Figure 9(d)). Figures 9(e) and 9(g) depict the fracture surfaces of the LTHP and super beta HIP specimens, respectively. In these cases, fatigue striations are seen emanating directly from the chamfers. Fractography results have identified two distinct failure mechanisms. The first involves defects serving as fatigue crack initiation (FCI) sites. The second mechanism is characterized by the formation of facets within the α phase of titanium, a notable microstructural feature. According to literature [28,55], microstructural features such as the one mentioned above acting as FCI are directly related to the α + β microstructures produced by the HIP treatments.

These findings suggest that the initiation and propagation of fatigue cracks in these specimens are influenced by the specific HIP cycle and its impact on the material's microstructure and surface features. The observations emphasize the role of HIP treatment in altering fatigue behavior by modifying defect characteristics and crack initiation sites.

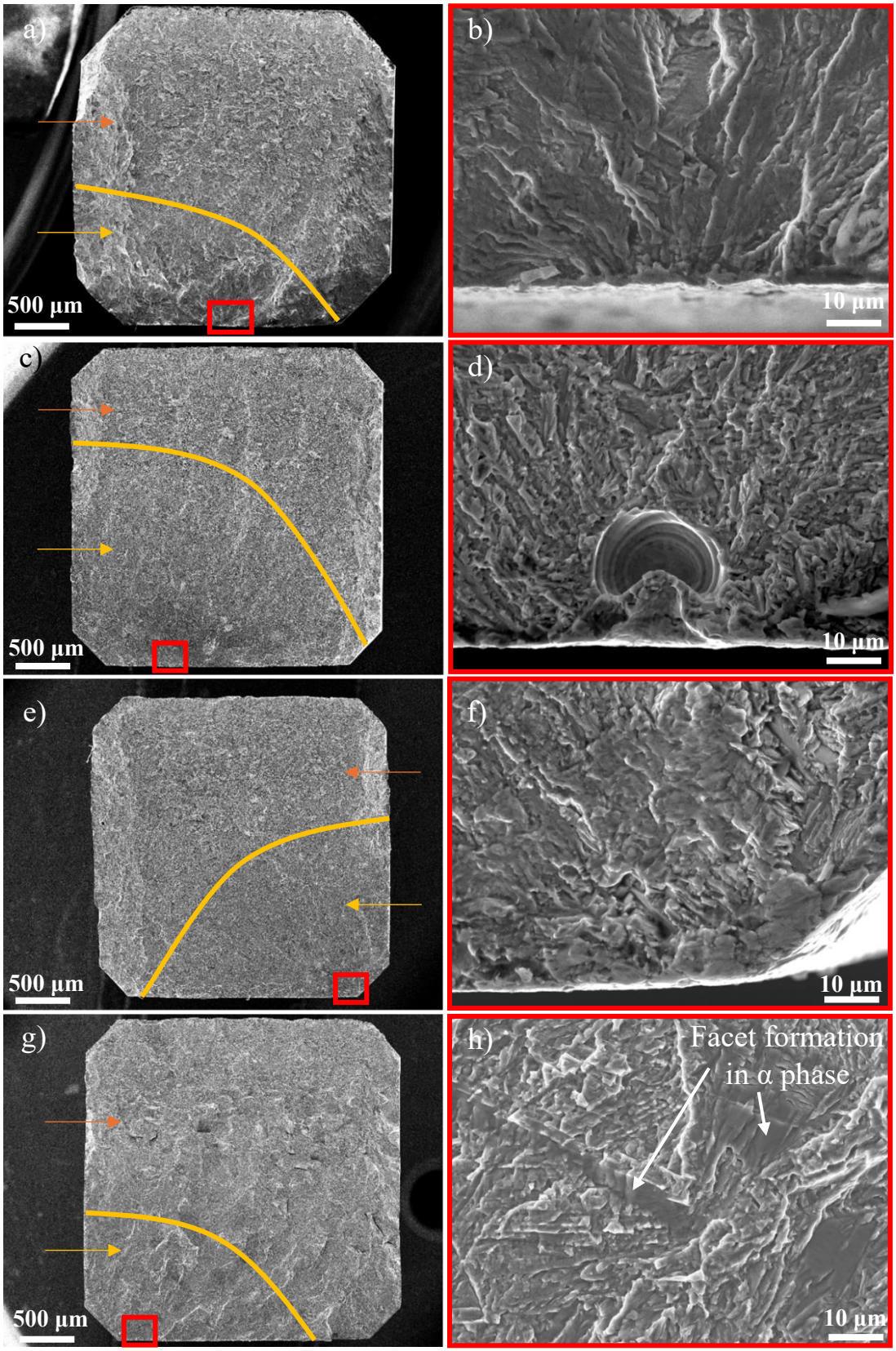

Figure 9. 4-point bending fatigue fracture morphology. a) Annealed. b) Standard HIP. c) LTHP HIP. d) Super Beta HIP.

4. Summary & Conclusion

This study analyzed and compared the fatigue behavior of 4-point bending Ti-6Al-4V specimens manufactured by L-PBF and subjected to various heat treatments. Specimens were tested under different conditions, including annealed heat treatment and three HIP cycles: standard, low temperature/high pressure (LTHP), and super beta. Additionally, the study examined microstructural characterization, mechanical properties, fatigue behavior, and its corresponding fracture surfaces.

Significant conclusions in this study include the following:

- The microstructure evolved in response to different heat treatments, showing the presence of α' martensite, thin and coarse α platelets, prior-β grains elongated along the build direction, and coarse equiaxed prior-β grains.
- The annealed heat treatment group exhibited the highest values for yield strength, ultimate tensile strength, and hardness. The HIP treatment groups enhanced the ductility of the specimens.
- Among the HIP treatment groups, the LTHP process demonstrated the best fatigue performance, followed by the standard and super beta HIP groups.
- Both the microstructure and HIP cycle parameters significantly influence fatigue behavior.
- Fractography results revealed two primary failure mechanisms at the FCI sites: defect-related and microstructural feature-related, with the latter being more dominant.

Acknowledgements

All research presented in this paper was carried out at The University of Texas at El Paso (UTEP) within the W.M. Keck Center for 3D Innovation (Keck Center). The authors extend their gratitude to NASA for funding the NASA ULI project (Grant 80NSSC19M0123), enabling our organization to conduct this research. Special thanks are also extended to Chad Beamer and Quintus Technologies for performing the HIP treatments, and to Dr. Tin and Michael Edward for their assistance with the EBSD analysis of the specimens.

Conflicts of Interest: The authors declare no conflict of interest.

References

[1] Harun WSW, Manam NS, Kamariah MSIN, Sharif S, Zulkifly AH, Ahmad I, et al. A review of powdered additive manufacturing techniques for Ti-6al-4v biomedical applications. Powder Technology 2018;331:74–97. https://doi.org/10.1016/j.powtec.2018.03.010.

[2] Liu Z, He B, Lyu T, Zou Y. A Review on Additive Manufacturing of Titanium Alloys for Aerospace Applications: Directed Energy Deposition and Beyond Ti-6Al-4V. JOM 2021;73:1804–18. https://doi.org/10.1007/s11837-021-04670-6.

[3] Shi H, Zhou P, Li J, Liu C, Wang L. Functional Gradient Metallic Biomaterials: Techniques, Current Scenery, and Future Prospects in the Biomedical Field. Front Bioeng Biotechnol 2021;8:616845. https://doi.org/10.3389/fbioe.2020.616845.

[4] Dev Singh D, Arjula S, Raji Reddy A. Functionally Graded Materials Manufactured by Direct Energy Deposition: A review. Materials Today: Proceedings 2021;47:2450–6. https://doi.org/10.1016/j.matpr.2021.04.536.

[5] Salmi M. Additive Manufacturing Processes in Medical Applications. Materials (Basel) 2021;14:191. https://doi.org/10.3390/ma14010191.

[6] Nabil ST, Banuelos C, Ramirez B, Cruz A, Watanabe KI, Arrieta E, et al. Exploring IN718 Alloy Production with Bi-directional Raster and Stochastic spot Melting Techniques using an Open-source Electron Beam Melting System, University of Texas at Austin; 2023. https://doi.org/10.26153/tsw/50954.
[7] Diaz JC, Watanabe K, Rubio A, De La Cruz A, Godinez D, Nabil ST, et al. Effect of Layer Thickness and Heat Treatment on Microstructure and Mechanical Properties of Alloy 625 Manufactured by Electron Beam Powder Bed Fusion. Materials 2022;15:7767. https://doi.org/10.3390/ma15217767.
[8] Chowdhury S, Yadaiah N, Prakash C, Ramakrishna S, Dixit S, Gupta LR, et al. Laser powder bed fusion: a state-of-the-art review of the technology, materials, properties & defects, and numerical modelling. Journal of Materials Research and Technology 2022;20:2109–72. https://doi.org/10.1016/j.jmrt.2022.07.121.
[9] Ladani L, Sadeghilaridjani M. Review of Powder Bed Fusion Additive Manufacturing for Metals. Metals 2021;11:1391. https://doi.org/10.3390/met11091391.
[10] Molotnikov A, Kingsbury A, Brandt M. Current state and future trends in laser powder bed fusion technology. Fundamentals of Laser Powder Bed Fusion of Metals, Elsevier; 2021, p. 621–34. https://doi.org/10.1016/B978-0-12-824090-8.00011-1.
[11] Nabil ST, Arrieta E, Wicker RB, Benedict M, Medina F. Effect of Thermal Aging in the Fatigue Life of Hot Isostatic Pressed AlSi10Mg Fabricated by Laser Powder Bed Fusion. 2022 International Solid Freeform Fabrication Symposium, 2022. http://dx.doi.org/10.26153/tsw/44562.
[12] Mandev YZ, Mandev E, Yetim AF. Effects of Laser Powder Bed Fusion Process Parameters on Porosity, Liquid Retention, and Thermal and Surface Properties for 316L, CoCrW and Ti6Al4V Alloys. J of Materi Eng and Perform 2024. https://doi.org/10.1007/s11665-024-09381-y.
[13] Nabavi SF, Dalir H, Farshidianfar A. A comprehensive review of recent advances in laser powder bed fusion characteristics modeling: metallurgical and defects. Int J Adv Manuf Technol 2024;132:2233–69. https://doi.org/10.1007/s00170-024-13491-1.
[14] Narra SP, Rollett AD, Ngo A, Scannapieco D, Shahabi M, Reddy T, et al. Process qualification of laser powder bed fusion based on processing-defect structure-fatigue properties in Ti-6Al-4V. Journal of Materials Processing Technology 2023;311:117775. https://doi.org/10.1016/j.jmatprotec.2022.117775.
[15] Cunningham R, Nicolas A, Madsen J, Fodran E, Anagnostou E, Sangid MD, et al. Analyzing the effects of powder and post-processing on porosity and properties of electron beam melted Ti-6Al-4V. Materials Research Letters 2017;5:516–25. https://doi.org/10.1080/21663831.2017.1340911.
[16] Alegre JM, Díaz A, García R, Peral LB, Cuesta II. Effect of HIP post-processing at 850 °C/200 MPa in the fatigue behavior of Ti-6Al-4V alloy fabricated by Selective Laser Melting. International Journal of Fatigue 2022;163:107097. https://doi.org/10.1016/j.ijfatigue.2022.107097.
[17] Wycisk E, Solbach A, Siddique S, Herzog D, Walther F, Emmelmann C. Effects of Defects in Laser Additive Manufactured Ti-6Al-4V on Fatigue Properties. Physics Procedia 2014;56:371–8. https://doi.org/10.1016/j.phpro.2014.08.120.
[18] Li P, Warner DH, Fatemi A, Phan N. Critical assessment of the fatigue performance of additively manufactured Ti–6Al–4V and perspective for future research. International Journal of Fatigue 2016;85:130–43. https://doi.org/10.1016/j.ijfatigue.2015.12.003.
[19] Gong H, Rafi K, Gu H, Janaki Ram GD, Starr T, Stucker B. Influence of defects on mechanical properties of Ti–6Al–4V components produced by selective laser melting and electron beam melting. Materials & Design 2015;86:545–54. https://doi.org/10.1016/j.matdes.2015.07.147.
[20] du Plessis A, Macdonald E. Hot isostatic pressing in metal additive manufacturing: X-ray tomography reveals details of pore closure. Additive Manufacturing 2020;34:101191. https://doi.org/10.1016/j.addma.2020.101191.
[21] Jamhari FI, Foudzi FM, Buhairi MA. Effect of HIP on Porosity of Ti6Al4V Manufactured by Laser Powder Bed Fusion: A Brief Review. In: Abdollah MFB, Amiruddin H, Phuman Singh AS, Abdul Munir F, Ibrahim A, editors. Proceedings of the 7th International Conference and Exhibition on

Sustainable Energy and Advanced Materials (ICE-SEAM 2021), Melaka, Malaysia, Singapore: Springer Nature; 2022, p. 22–5. https://doi.org/10.1007/978-981-19-3179-6_5.
[22] Andrew Hills M, Scott Malcolm J, Mohamed Dhansay N, Hermann Becker T. High cycle fatigue strength of hot isostatically pressed and chemically etched laser powder bed fusion produced Ti-6Al-4V. International Journal of Fatigue 2023;175:107774. https://doi.org/10.1016/j.ijfatigue.2023.107774.
[23] Zhao X, Li S, Zhang M, Liu Y, Sercombe TB, Wang S, et al. Comparison of the microstructures and mechanical properties of Ti–6Al–4V fabricated by selective laser melting and electron beam melting. Materials & Design 2016;95:21–31. https://doi.org/10.1016/j.matdes.2015.12.135.
[24] Yu H, Li F, Wang Z, Zeng X. Fatigue performances of selective laser melted Ti-6Al-4V alloy: Influence of surface finishing, hot isostatic pressing and heat treatments. International Journal of Fatigue 2019;120:175–83. https://doi.org/10.1016/j.ijfatigue.2018.11.019.
[25] Moran TP, Carrion PE, Lee S, Shamsaei N, Phan N, Warner DH. Hot Isostatic Pressing for Fatigue Critical Additively Manufactured Ti-6Al-4V. Materials (Basel) 2022;15:2051. https://doi.org/10.3390/ma15062051.
[26] Kasperovich G, Hausmann J. Improvement of fatigue resistance and ductility of TiAl6V4 processed by selective laser melting. Journal of Materials Processing Technology 2015;220:202–14. https://doi.org/10.1016/j.jmatprotec.2015.01.025.
[27] Greitemeier D, Palm F, Syassen F, Melz T. Fatigue performance of additive manufactured TiAl6V4 using electron and laser beam melting. International Journal of Fatigue 2017;94:211–7. https://doi.org/10.1016/j.ijfatigue.2016.05.001.
[28] Bhandari L, Gaur V. Different post-processing methods to improve fatigue properties of additively built Ti-6Al-4V alloy. International Journal of Fatigue 2023;176:107850. https://doi.org/10.1016/j.ijfatigue.2023.107850.
[29] Leuders S, Thöne M, Riemer A, Niendorf T, Tröster T, Richard HA, et al. On the mechanical behaviour of titanium alloy TiAl6V4 manufactured by selective laser melting: Fatigue resistance and crack growth performance. International Journal of Fatigue 2013;48:300–7. https://doi.org/10.1016/j.ijfatigue.2012.11.011.
[30] Naab B, Celikin M. The role of microstructural evolution on the fatigue behavior of additively manufactured Ti–6Al–4V alloy. Materials Science and Engineering: A 2022;859:144232. https://doi.org/10.1016/j.msea.2022.144232.
[31] Kahlin M, Ansell H, Moverare JJ. Fatigue behaviour of notched additive manufactured Ti6Al4V with as-built surfaces. International Journal of Fatigue 2017;101:51–60. https://doi.org/10.1016/j.ijfatigue.2017.04.009.
[32] Kahlin M, Ansell H, Basu D, Kerwin A, Newton L, Smith B, et al. Improved fatigue strength of additively manufactured Ti6Al4V by surface post processing. International Journal of Fatigue 2020;134:105497. https://doi.org/10.1016/j.ijfatigue.2020.105497.
[33] Rafi HK, Karthik NV, Gong H, Starr TL, Stucker BE. Microstructures and Mechanical Properties of Ti6Al4V Parts Fabricated by Selective Laser Melting and Electron Beam Melting. J of Materi Eng and Perform 2013;22:3872–83. https://doi.org/10.1007/s11665-013-0658-0.
[34] Lv Z, Li H, Che L, Chen S, Zhang P, He J, et al. Effects of HIP Process Parameters on Microstructure and Mechanical Properties of Ti-6Al-4V Fabricated by SLM. Metals 2023;13:991. https://doi.org/10.3390/met13050991.
[35] Benedetti M, Fontanari V, Bandini M, Zanini F, Carmignato S. Low- and high-cycle fatigue resistance of Ti-6Al-4V ELI additively manufactured via selective laser melting: Mean stress and defect sensitivity. International Journal of Fatigue 2018;107:96–109. https://doi.org/10.1016/j.ijfatigue.2017.10.021.
[36] Pegues JW, Shao S, Shamsaei N, Sanaei N, Fatemi A, Warner DH, et al. Fatigue of additive manufactured Ti-6Al-4V, Part I: The effects of powder feedstock, manufacturing, and post-process conditions on the resulting microstructure and defects. International Journal of Fatigue 2020;132:105358. https://doi.org/10.1016/j.ijfatigue.2019.105358.

[37] Benedetti M, Torresani E, Leoni M, Fontanari V, Bandini M, Pederzolli C, et al. The effect of post-sintering treatments on the fatigue and biological behavior of Ti-6Al-4V ELI parts made by selective laser melting. Journal of the Mechanical Behavior of Biomedical Materials 2017;71:295–306. https://doi.org/10.1016/j.jmbbm.2017.03.024.
[38] Varela J, Arrieta E, Paliwal M, Marucci M, Sandoval JH, Gonzalez JA, et al. Investigation of Microstructure and Mechanical Properties for Ti-6Al-4V Alloy Parts Produced Using Non-Spherical Precursor Powder by Laser Powder Bed Fusion. Materials 2021;14:3028. https://doi.org/10.3390/ma14113028.
[39] Liu S, Shin YC. Additive manufacturing of Ti6Al4V alloy: A review. Materials & Design 2019;164:107552. https://doi.org/10.1016/j.matdes.2018.107552.
[40] Benzing J, Hrabe N, Quinn T, White R, Rentz R, Ahlfors M. Hot isostatic pressing (HIP) to achieve isotropic microstructure and retain as-built strength in an additive manufacturing titanium alloy (Ti-6Al-4V). Materials Letters 2019;257:126690. https://doi.org/10.1016/j.matlet.2019.126690.
[41] Titanium. Berlin, Heidelberg: Springer; 2007. https://doi.org/10.1007/978-3-540-73036-1.
[42] Vilaro T, Colin C, Bartout JD. As-Fabricated and Heat-Treated Microstructures of the Ti-6Al-4V Alloy Processed by Selective Laser Melting. Metall Mater Trans A 2011;42:3190–9. https://doi.org/10.1007/s11661-011-0731-y.
[43] Kobayashi S, Yang W, Tomobe Y, Okada R, Tsurekawa S. Low-angle boundary engineering for improving high-cycle fatigue property of 430 ferritic stainless steel. J Mater Sci 2020;55:9273–85. https://doi.org/10.1007/s10853-020-04555-0.
[44] Yan Q, Chen B, Kang N, Lin X, Lv S, Kondoh K, et al. Comparison study on microstructure and mechanical properties of Ti-6Al-4V alloys fabricated by powder-based selective-laser-melting and sintering methods. Materials Characterization 2020;164:110358. https://doi.org/10.1016/j.matchar.2020.110358.
[45] Murr LE, Quinones SA, Gaytan SM, Lopez MI, Rodela A, Martinez EY, et al. Microstructure and mechanical behavior of Ti–6Al–4V produced by rapid-layer manufacturing, for biomedical applications. Journal of the Mechanical Behavior of Biomedical Materials 2009;2:20–32. https://doi.org/10.1016/j.jmbbm.2008.05.004.
[46] Wang Q, Han C, Choma T, Wei Q, Yan C, Song B, et al. Effect of Nb content on microstructure, property and in vitro apatite-forming capability of Ti-Nb alloys fabricated via selective laser melting. Materials & Design 2017;126:268–77. https://doi.org/10.1016/j.matdes.2017.04.026.
[47] Eshawish N, Malinov S, Sha W, Walls P. Microstructure and Mechanical Properties of Ti-6Al-4V Manufactured by Selective Laser Melting after Stress Relieving, Hot Isostatic Pressing Treatment, and Post-Heat Treatment. J of Materi Eng and Perform 2021;30:5290–6. https://doi.org/10.1007/s11665-021-05753-w.
[48] Sterling A, Shamsaei N, Torries B, Thompson SM. Fatigue Behaviour of Additively Manufactured Ti-6Al-4 V. Procedia Engineering 2015;133:576–89. https://doi.org/10.1016/j.proeng.2015.12.632.
[49] Palanivel S, Dutt AK, Faierson EJ, Mishra RS. Spatially dependent properties in a laser additive manufactured Ti–6Al–4V component. Materials Science and Engineering: A 2016;654:39–52. https://doi.org/10.1016/j.msea.2015.12.021.
[50] Hinderdael M, Strantza M, De Baere D, Devesse W, De Graeve I, Terryn H, et al. Fatigue Performance of Ti-6Al-4V Additively Manufactured Specimens with Integrated Capillaries of an Embedded Structural Health Monitoring System. Materials 2017;10:993. https://doi.org/10.3390/ma10090993.
[51] Wu M-W, Lai P-H. The positive effect of hot isostatic pressing on improving the anisotropies of bending and impact properties in selective laser melted Ti-6Al-4V alloy. Materials Science and Engineering: A 2016;658:429–38. https://doi.org/10.1016/j.msea.2016.02.023.
[52] Leuders S, Vollmer M, Brenne F, Tröster T, Niendorf T. Fatigue Strength Prediction for Titanium Alloy TiAl6V4 Manufactured by Selective Laser Melting. Metall Mater Trans A 2015;46:3816–23. https://doi.org/10.1007/s11661-015-2864-x.

[53] Beretta S, Murakami Y. Statistical Analysis of Defects for Fatigue Strength Prediction and Quality Control of Materials. Fatigue & Fracture of Engineering Materials & Structures 1998;21:1049–65. https://doi.org/10.1046/j.1460-2695.1998.00104.x.
[54] Xu W, Sun S, Elambasseril J, Liu Q, Brandt M, Qian M. Ti-6Al-4V Additively Manufactured by Selective Laser Melting with Superior Mechanical Properties. JOM 2015;67:668–73. https://doi.org/10.1007/s11837-015-1297-8.
[55] Bache MR. Processing titanium alloys for optimum fatigue performance. International Journal of Fatigue 1999;21:S105–11. https://doi.org/10.1016/S0142-1123(99)00061-4.